Effect of Tb^{3+} concentration on the structure and optical properties of triply doped $ZnAl_2O_4$:1% Ce^{3+},1% Eu^{3+},x% Tb^{3+} nano-phosphors synthesized via citrate sol-gel method

S. V. Motloung[1*], K. G. Tshabalala[2], R. E. Kroon[3], T. T. Hlatshwayo[4], M. Mlambo[4], S. Mpelane[5]

[1]Department of Physics, Nelson Mandela University, P. O. Box 77000, Port Elizabeth 6031, South Africa

[2]Department of Physics, University of the Free State (Qwaqwa Campus), Private Bag X13, Phuthaditjhaba, 9866, South Africa

[3]Department of Physics, University of the Free State, P.O. Box 339, Bloemfontein, 9300, South Africa

[4]Department of Physics, University of Pretoria, Pretoria, 0002, South Africa

[5]Department of Chemistry, University of Johannesburg, P.O. Box: 524, Auckland Park, 2006, South Africa

Corresponding author:

Tel:+27 72 920 4758. E-mail: cchataa@gmail.com (Setumo Victor Motloung)

Highlights

• Ce^{3+}, Eu^{3+} and Tb^{3+} doped and triple doped $ZnAl_2O_4$ nano-powders were successfully synthesized via the citrate sol-gel method.
• Energy dispersive X-ray spectroscopy (EDS) results confirmed that the samples were made up of Zn, Al, O, Ce, Eu and Tb ions.
• The transmission electron microscopy (TEM) results confirmed that the prepared powders were in the nano-region.
• The ultraviolet–visible (UV–vis) spectra showed that different dopants and concentrations of Tb^{3+} influenced the bandgap of the host material.
• The photoluminescence (PL) results showed that there are emissions peaks from each dopant.

Abstract:

Ce^{3+}, Eu^{3+} and Tb^{3+} singly and triply doped $ZnAl_2O_4$ nano-powders were successfully synthesized via the citrate sol-gel method. X-ray diffraction (XRD) analysis showed that the powder samples consisted of the cubic crystalline phase. Energy dispersive X-ray spectroscopy (EDS) results confirmed the presence of all expected elements and the EDS map showed that the foreign ions were distributed homogeneously on the surface. Scanning electron microscopy (SEM) results revealed that the prepared powder morphology was influenced by doping. The transmission electron microscopy (TEM) results confirmed that the prepared powders were in the nano-scale region. The ultraviolet-visible (UV-vis) spectra showed that different

dopants and varying the Tb^{3+} concentration influenced the effective band gap (E_g) of the host. The photoluminescence (PL) results showed that the emission at 395 nm was due to the defects emission within the host material. Ce^{3+} doped samples showed a broad emission peak centered at 425 nm which is attributed to the 5d → 4f transition of Ce^{3+} ions. The sample doped with Eu^{3+} showed two emission peaks at 592 and 616 nm ascribed to the $^5D_0 \rightarrow {}^7F_1$ and $^5D_0 \rightarrow {}^7F_2$ transitions of Eu^{3+} ions, respectively. Tb^{3+} singly-doped sample showed four peaks located at 489, 545, 587 and 616 nm, which were respectively ascribed to $^5D_4 \rightarrow {}^7F_6$, $^7F_5$, $^7F_4$ and $^7F_3$ transitions of Tb^{3+} ions. The Commission Internationale de l'Elcairage (CIE), or International Commission on Illumination, co-ordinates showed that the emission color could be tuned by varying the Tb^{3+} concentration.

Keywords: Sol-gel, Triple Doped, Zinc Aluminate, Luminescence

1. Introduction

Zinc aluminate ($ZnAl_2O_4$) is a polycrystalline material belonging to a family of compounds known as spinel-type oxides [1]. $ZnAl_2O_4$ is known to be a wide-band gap semiconductor with the optical band gap (E_g) of 3.8 eV. $ZnAl_2O_4$ has other fascinating properties such as chemical inertness, thermal stability and high mechanical resistance which makes it suitable for a lot of applications including optical coating, host matrix and photoelectronic devices [2]. $ZnAl_2O_4$ is a binary compound which is generally noted as AB_2O_4, where A (Zn^{2+}) is a divalent ion occupying the tetrahedral site (T_d) and B (Al^{3+}) is a trivalent ion occupying the octahedral site (O_h).

Numerous synthesis methods for nanophosphors have been developed over the years, such as co-precipitation [3], pyrolysis [4], solvothermal [5], combustion [6], citrate sol-gel [7] and have been used to synthesize pure and doped $ZnAl_2O_4$ phosphors. In this work, the citrate sol-gel method has been adopted due to its advantages of being relatively cheap, good in controlling the stoichiometry, producing samples with high homogeneity, low-temperature processing and its ability to produce nanostructured powders [8]. $ZnAl_2O_4$ has been reported in literature to be activated by rare earth (RE) [9,10], transition metal [11] and post transition metal [12] ions. For an example, Tshabalala et al. [9] have shown that $ZnAl_2O_4$:Ce^{3+} can produce blue emissions, which were attributed to $^5D_1 \rightarrow {}^2F_{(7/2+5/2)}$ multiplets in the Ce^{3+} ions. Fernandez-Osorio et al. [13] have shown that $ZnAl_2O_4$:Eu^{3+} phosphors can be used where red emissions is required. The red emission was attributed to be due to $^5D_0 \rightarrow {}^7F_2$ transitions in the Eu^{3+} ions. Omkaram et al. [14] have shown that Tb^{3+} can be used to form a green emitting phosphor due to $^5D_4 \rightarrow {}^7F_5$ transitions in the Tb^{3+} ions. Chengaiah et al. [15] investigated Ce^{3+} and Eu^{3+} co-doped $Na_3Gd(PO)_2$ and the results showed that

the luminescent colors of $Na_3Gd(PO)_2:Ce^{3+}$, Eu^{3+} can be varied from red to blue by varying the concentration of the Ce^{3+} ions. Motloung et al. [10] have shown that the luminescent colors of the $ZnAl_2O_4:Ce^{3+},Eu^{3+}$ system can be varied from blue to red by varying the concentration of the Eu^{3+} ions. From these previous studies focused on the $ZnAl_2O_4$ host material, it can be seen that it is possible to single dope [11,12,14] and co-dope [10,15] the $ZnAl_2O_4$ lattice with different foreign atoms. However, as far as the third degree of doping (or triply doped) is concerned, there has never been a study on $ZnAl_2O_4$ that has been reported from the literature. Thus, the purpose of the current study is to extensively investigate $ZnAl_2O_4$:1% Ce^{3+},1% Eu^{3+},x% Tb^{3+} ($0 < x \leq 2.4$) in order to acquire a deeper insight into the materials nature of $ZnAl_2O_4$ with the initial aim of producing more promising oxides for the white light emitting phosphors (WLEP) material by mixing the blue (Ce^{3+}), green (Tb^{3+}) and red (Eu^{3+}) emitting foreign ions. However, our results revealed that the prepared phosphor materials emit dominantly a green colour. The emission pathways associated with the observed emissions is also discussed in detail.

2. Experimental

Un-doped ($ZnAl_2O_4$), singly doped (with 1% Ce^{3+}, 1% Eu^{3+} and 1% Tb^{3+}) and triply doped nano-powders were synthesized using a well-known citrate sol–gel technique [16]. $Zn(NO_3)_2{\cdot}6H_2O$ (98%) and $Al(NO_3)_3{\cdot}9H_2O$ (98.5%) were dissolved in deionized water. The sols stoichiometric molar ratio of Zn:Al was 2:1. Specified amounts of $Ce(NO_3)_3{\cdot}6H_2O$ (99.9%), $Eu(NO_3)_3{\cdot}5H_2O$ (99.9%) and $Tb(NO_3)_3{\cdot}6H_2O$ (99.9%) were added into separate beakers of the solution in order to single dope $ZnAl_2O_4$ with 1% Ce^{3+}, 1% Eu^{3+} and 1% Tb^{3+}, respectively. These impurities concentration were chosen because they resulted on the optimum luminescence intensities in references [9,13,14]. A similar procedure was then followed for the triple-doping where the concentrations of Ce^{3+} and Eu^{3+} ions were kept constant at 1 %, while the molar concentration of Tb^{3+} ions was varied in the range ($0 < x \leq 2.4$) mol%. Citric acid (CA), $C_8H_8O_7{\cdot}H_2O$ (99%), was used as a chelating agent and the Zn:CA molar ratio was kept constant at 1:0.75 for all samples. The heating temperature was kept at ~ 80 °C while constantly stirring using a magnetic stirrer until gels were formed. The gels were dried in an oven kept at a temperature of 130 °C for 1 h and ground into fine powders by using mortar and pestle. The dried sample powders were subsequently annealed at 800 °C in a furnace for 1 h.

The crystal structure of the prepared nano-powders was analyzed by X-ray diffraction (XRD) using a Bruker D8-Advance system with Cu Kα X-rays of wavelength 0.154050 nm. The surface morphology and the elementary composition were investigated using Shimadzu Superscan ZU SXX-550 electron microscope (SEM) coupled with an energy dispersive X-ray spectroscope (EDS). Transmission electron microscopy (TEM) was performed by JEOL JEM 2100 transmission electron microscopy. The diffuse

reflectance spectra of the samples were measured using a UV-vis spectrophotometer (UV-2550). The room temperature photoluminescence (PL) measurements were performed with a Hitachi F-7000 fluorescence spectrophotometer using a monochromatized xenon lamp as an excitation source. Further PL and lifetime measurements were made using an Edinburgh Instruments FLS980 system.

3. Results and discussion

3.1 X-ray diffraction analysis

Fig. 1 shows the XRD patterns of (a) the host, 1% Ce^{3+}, 1% Eu^{3+}, 1% Tb^{3+} singly doped samples and (b) the triply doped samples. The samples are polycrystalline and their diffraction patterns matched perfectly well with the standard pattern of the cubic $ZnAl_2O_4$ spinel JCPDS No. 82-1043. There are no detectable traces of impurities such as ZnO, Al_2O_3 or any related Ce_2O_3, Eu_2O_3 and Tb_2O_3 from all the prepared samples. The crystallites sizes were estimated by Scherrer's equation [17] using the most intense peak (311) and the results are presented in Table 1. The results revealed that doping influences the crystallite size of the prepared nano-phosphors.

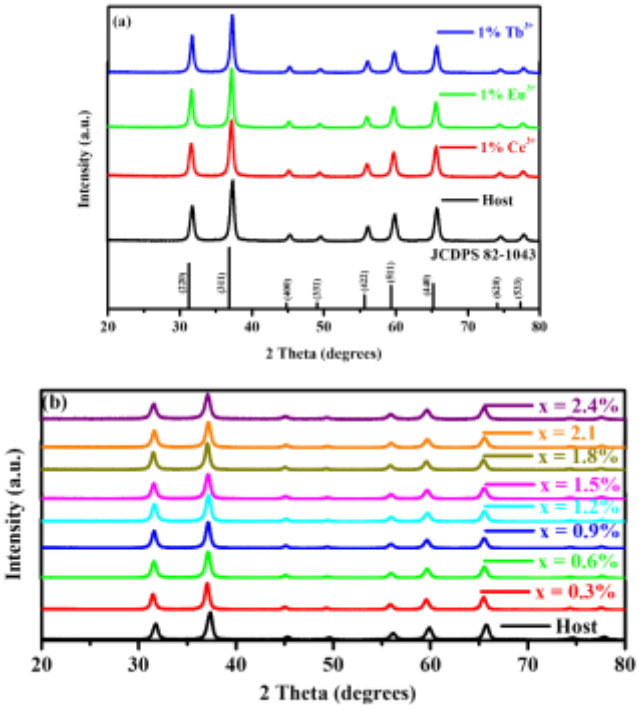

Fig. 1. The X-ray diffraction patterns of the (a) host and singly doped samples; and (b) the triply doped samples for varying Tb^{3+} concentration.

The most intense (311) diffraction peaks are illustrated in Fig. 2. The lattice parameter (*a*) for all samples are presented in Table 1. The value for the host material is very close to, and consistent with, those reported by Zawadzki et al. [18], Tshabalala et al. [9] and Motloung et al. [10]. Fig. 2 shows that there is a peak shift to the lower diffraction angle for the singly and triply doped samples in comparison to the host material and that implies an expansion of the lattice, which is due to the atomic radii of the dopants. The Ce^{3+}, Eu^{3+} and Tb^{3+} ions are expected to substitute Zn^{2+} and Al^{3+} ions in the $ZnAl_2O_4$ host matrix and since the ionic radii of Ce^{3+} (1.11 Å), Eu^{3+} (0.95 Å) [19] and Tb^{3+} (1.00 Å) [9] are larger than that of Zn^{2+}(0.74 Å) and Al^{3+}(0.50 Å) [20], their incorporation is expected to strain the lattice and expand its unit cell volume. This serves as the main reason for the general shift to the lower diffraction angle observed in Fig. 2 (a) and (b). These results are also confirmed by the calculated *a* values in Table 1. As anticipated, the lattice parameter *a* was observed to increase further (see Table 1) for the triply doped samples. This confirms that the foreign ions were successfully incorporated into the host material crystal structure. Both the decrease and increase in (311) diffraction peak intensity were observed in both Fig. 2 (a) and (b). This is linked to a change of the $ZnAl_2O_4$ crystal quality [21,22]. The decrease in diffraction intensity was attributed to the crystalline quality during the growth of $ZnAl_2O_4$ nanocrystals, while the increase in diffraction intensity was attributed to the enhancement of the crystalline quality [10]. Thus, it is clear that the type of dopant and varying the Tb^{3+} concentration on the triply doped samples influences the crystallinity.

Table 1. Summary of the sample identification, position of the (311) peak, crystallite size and lattice parameter.

Sample ID	2θ (degrees)	FWHM (mrad)	Crystallites size (nm)	a (nm)
Host	37.32	9.11 ± 0.01	16 ± 0.1	0.798 ± 0.003
1% Ce^{3+}	37.18	9.02 ± 0.03	16 ± 0.2	0.801 ± 0.003
1% Eu^{3+}	37.19	7.95 ± 0.07	18 ± 0.4	0.801 ± 0.001
1% Tb^{3+}	37.22	8.12 ± 0.08	18 ± 0.1	0.800 ± 0.003
x = 0.3	37.03	7.92 ± 0.06	18 ± 0.5	0.804 ± 0.003
x = 0.6	37.14	8.63 ± 0.06	17 ± 0.5	0.802 ± 0.001
x = 0.9	37.16	8.19 ± 0.06	18 ± 0.6	0.802 ± 0.002
x = 1.2	37.15	8.71 ± 0.08	17 ± 0.5	0.802 ± 0.001
x = 1.5	37.14	8.86 ± 0.06	17 ± 0.5	0.802 ± 0.003
x = 1.8	37.09	8.07 ± 0.07	18 ± 0.1	0.803 ± 0.003
x = 2.1	37.12	8.94 ± 0.04	16 ± 0.3	0.802 ± 0.003
x = 2.4	37.11	9.47 ± 0.07	15 ± 0.4	0.803 ± 0.006

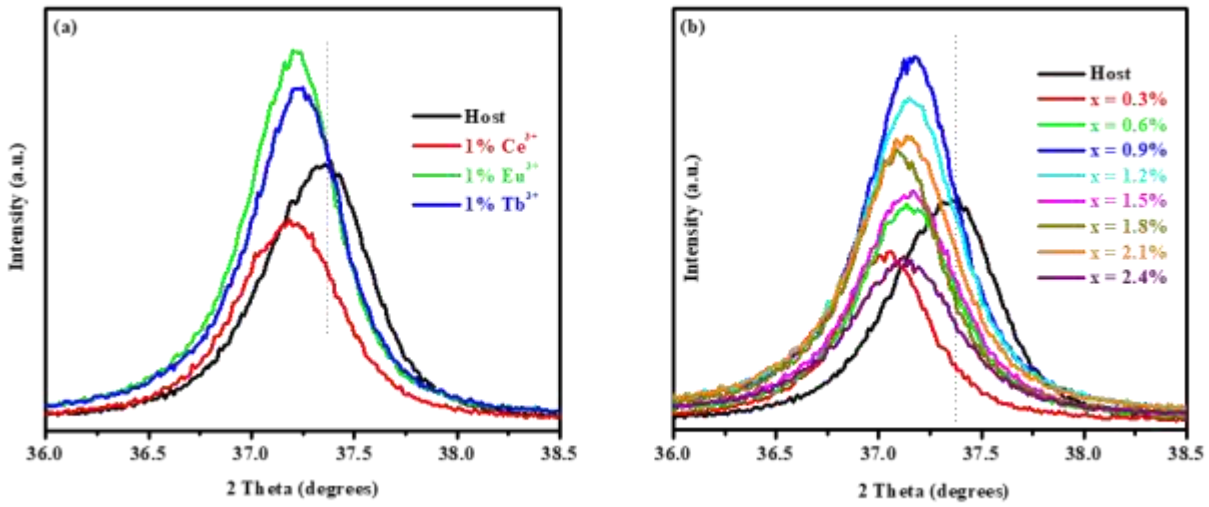

Fig. 2. The (311) diffraction peak for (a) the host and singly-doped samples; and (b) the triply doped samples for varying Tb^{3+} concentration ($0 < x \leq 2.4$).

3.2 Energy Dispersive X-ray Spectroscopy (EDS)

Fig. 3 shows the EDS spectra of the host, single and triple doped samples. In general, the analysis indicated the presence of the expected elementary composition Zn, Al, O, Ce, Eu and Tb. The carbon (C) peak observed is due to conductive carbon films coated on the sample holder during EDS measurements [23]. Fig. 4 presents the EDS mapping of the x = 1.8% triple doped samples. The map shows that the elements are uniform on the surface [24]. Thus, the results show that citrate sol-gel method is effective in incorporating dopant ions into the host matrix.

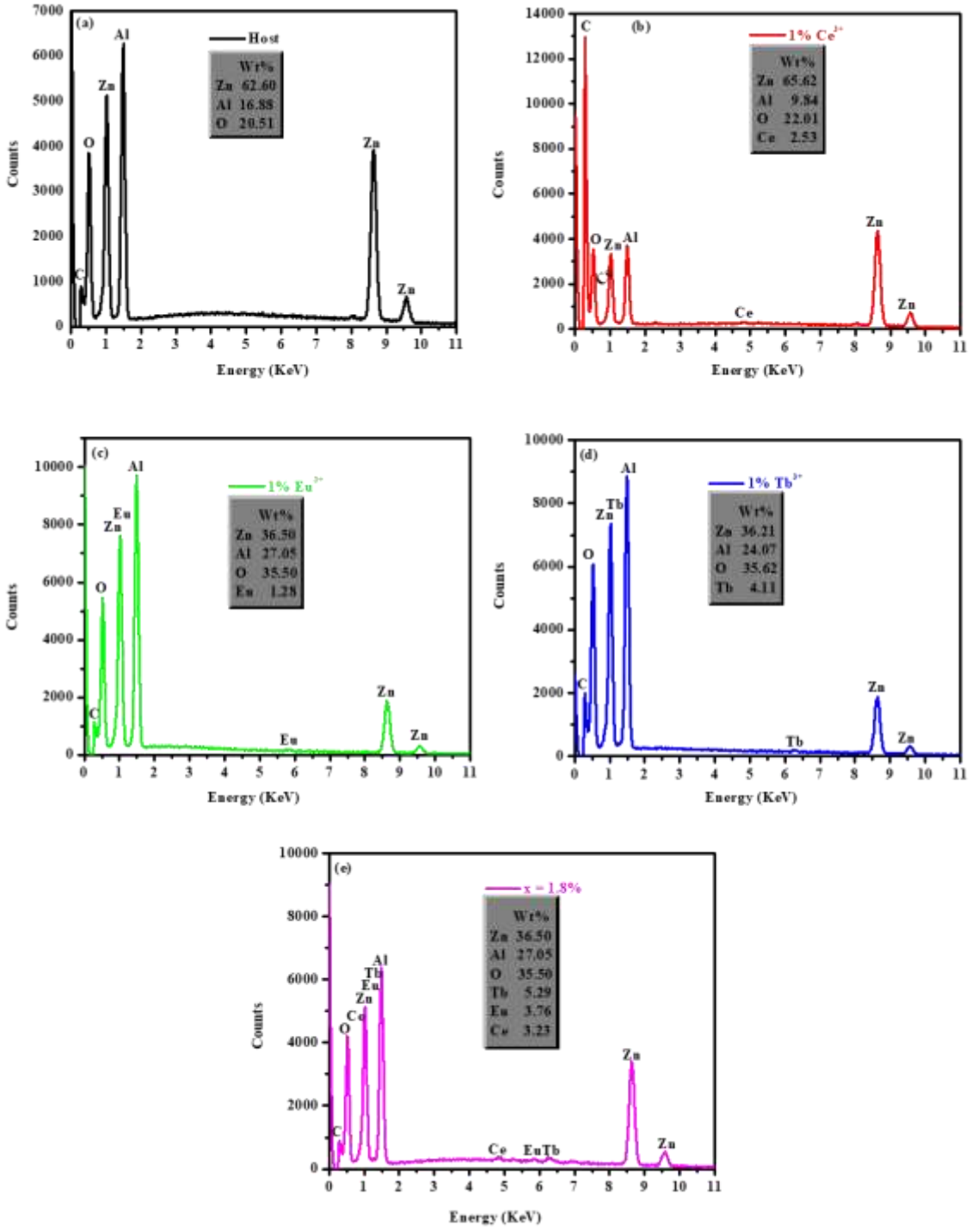

Fig. 3. EDS spectra of the (a) $ZnAl_2O_4$ (host) (b) 1% Ce^{3+}, (c) 1% Eu^{3+}, (d) 1% Tb^{3+} singly doped and (e) x = 1.8% Tb^{3+} triply doped samples.

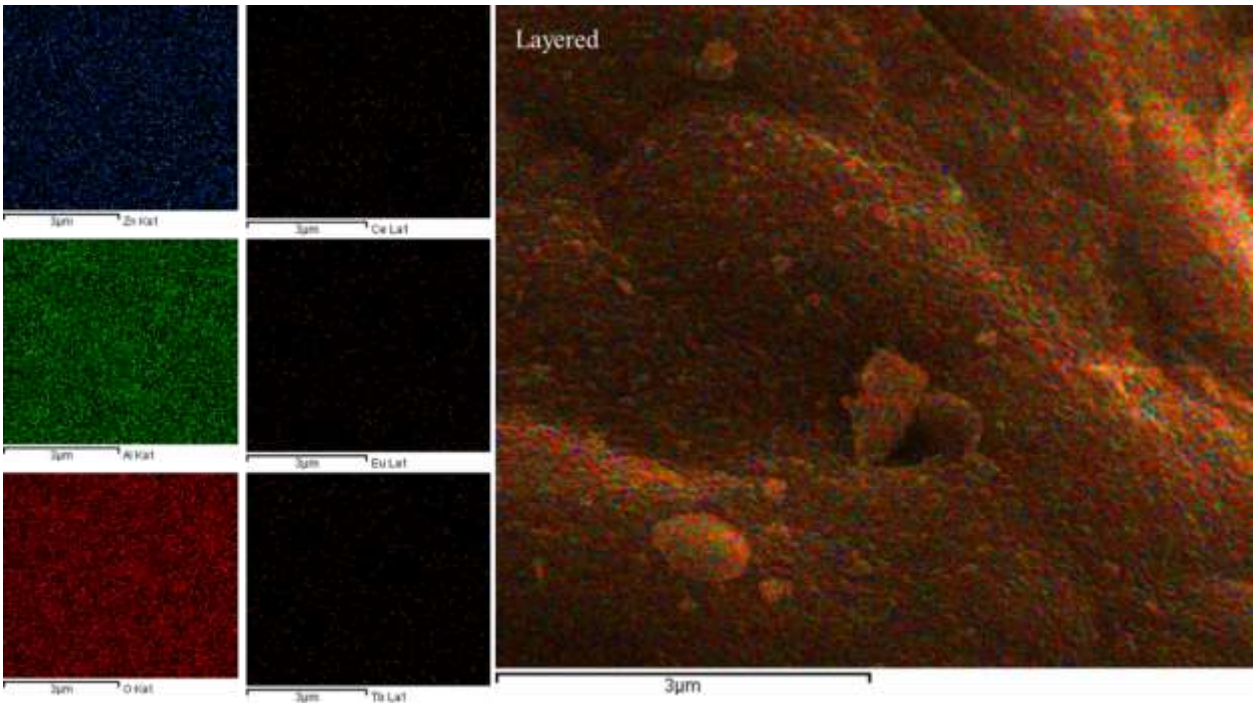

Fig. 4. EDS elemental mapping of the x = 1.8% sample.

3.3 Scanning electron microscopy (SEM) and Transmission electron microscopy (TEM)

SEM was used to study the surface morphology of the samples and the results are shown in Fig. 5. The morphology of the host (see Fig. 5 (a)) shows the small crystallites of irregular sizes, which are agglomerated together to make bigger crystallites. The Ce^{3+} doped sample shown in Fig. 5 (b) shows the stars-like crystallites distributed over the surface. The Eu^{3+} doped sample shown in Fig. 5 (c) shows the high degree of crystallites agglomeration with a rough surface and few irregular crystallites are distributed over the surface. Tb^{3+} doped sample shown in Fig. 5 (d) revealed the small crystallites distributed evenly over the surface. The sample triply doped at x = 1.8% Tb^{3+} presented in Fig. 5 (e) shows the agglomerated crystallites over the surface. The surface morphology seems to be rough like the one for the Eu^{3+} sample (see Fig. 5 (c)). Therefore, the results suggest that the morphology of the prepared powder is influenced by the dopant type and triply doping the host material.

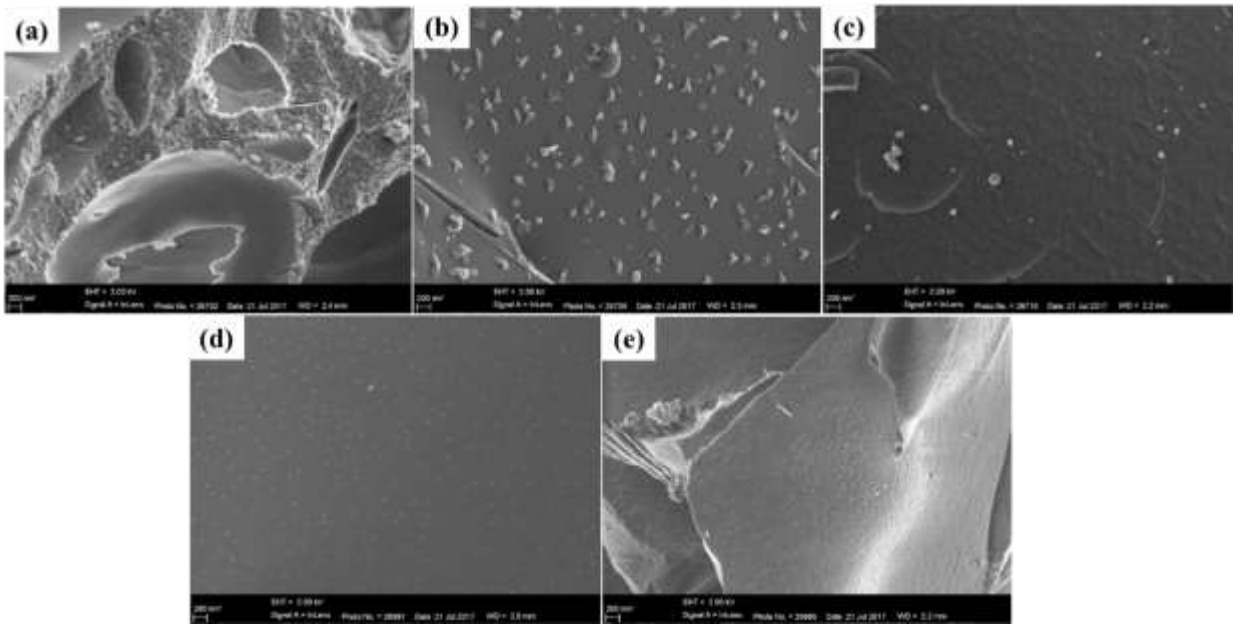

Fig. 5. SEM micrographs of (a) $ZnAl_2O_4$ (host), (b) 1% Ce^{3+}, (c) 1% Eu^{3+}, (d) 1% Tb^{3+} singly doped and (e) x = 1.8% triply doped sample.

The TEM results of the host, singly and triply doped (x = 1.8% Tb^{3+}) samples are displayed in Fig. 6. The average crystallite size was estimated to be around 20 nm which correlates with the average size estimated from the XRD results. The cubic-like crystallites can also be seen is some of these images which agrees very well with the cubic phase of the $ZnAl_2O_4$ spinel (JCPDS No. 82-1043) suggested by the XRD results. Crystallites agglomeration suggested by SEM is also observed in TEM results. The lattice fringes can also be observed in some of these images. Thus, it is clear that the citrate sol-gel method can produce powder containing nanoparticles. It is also evident that TEM, XRD and SEM results are in agreement with each other.

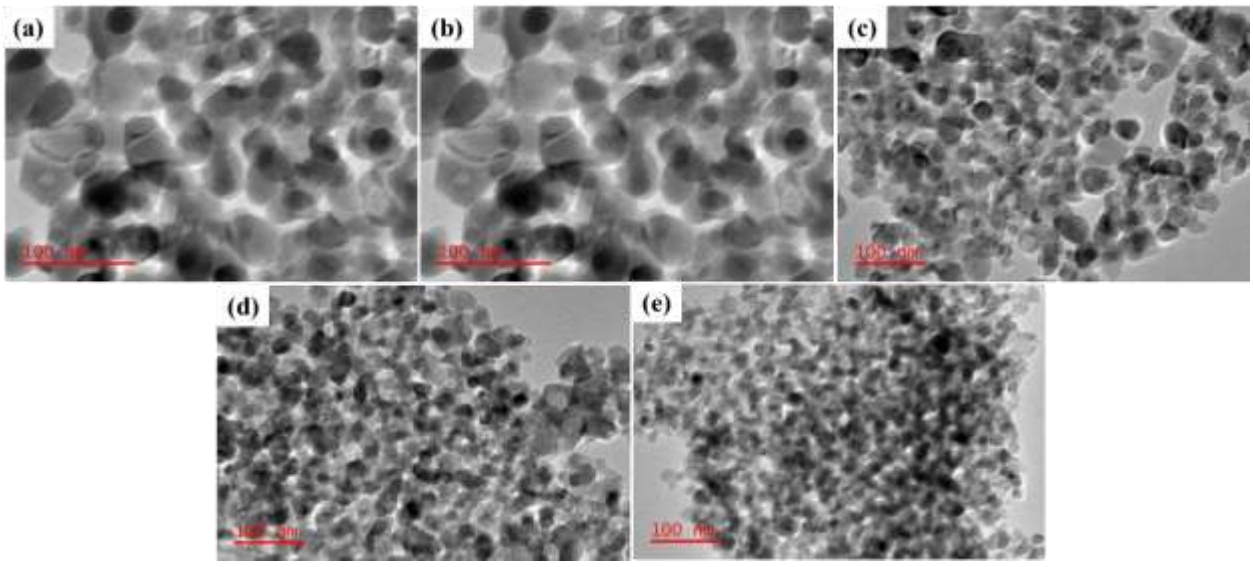

Fig. 6. TEM images of the (a) $ZnAl_2O_4$ (host), (b) 1% Ce^{3+}, (c) 1% Eu^{3+}, (d) 1% Tb^{3+} singly doped and (e) x = 1.8% triply doped sample.

3.4 Ultraviolet-Visible Spectroscopy

The characteristic absorption of the host and the effects of the Ce^{3+}, Eu^{3+} and Tb^{3+} dopants were investigated using UV-Vis diffuse reflection spectroscopy. Fig. 7 (a) and (b) shows the reflectance spectra of the $ZnAl_2O_4$ (host), singly and triply doped samples, respectively. The results revealed the presence of absorption bands at 234, 383 and 430 nm. The 234 nm absorption is certainly attributed to the band-to-band transitions in host material [25]. The nonsignificant band at 310 nm is attributed to the change of lamp to the other lamp on the UV-Vis system. The absorption band at 383 nm is due to defects absorption within the host material [8]. The Tb^{3+} and Eu^{3+} single doped samples revealed similar behavior to the host sample. However, for the Ce^{3+} doped sample, it is clear from Fig. 7 (a) that the absorption band at around 430 nm originated from Ce^{3+} ion [26]. The $ZnAl_2O_4$:1% Ce^{3+} and $ZnAl_2O_4$:1% Eu^{3+} samples showed lower reflectance percentage (or stronger absorption) compared to the host sample between 400 to 800 nm while the $ZnAl_2O_4$:1% Ce^{3+} showed a larger reflectance percentage for the same region. As shown in reflectance spectra in Fig. 7 (a), we propose that the large difference exhibited for $ZnAl_2O_4$:1% Ce^{3+} sample comparing to the others is due to the Ce^{3+} absorption. The triple doped samples shown in Fig. 7 (b) showed an increase in reflectance percentage associated with an increase in x% Tb^{3+} ions. Generally, these results shows that the dopant type and increasing the Tb^{3+} concentration on the triply doped samples influences the reflectance of host matrix.

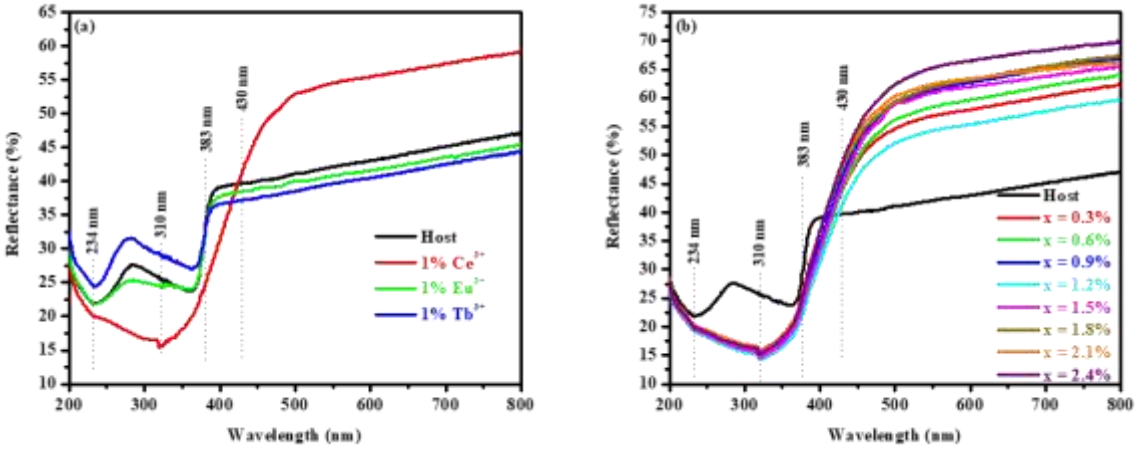

Fig. 7. The diffuse reflectance spectra of (a) $ZnAl_2O_4$ (host) and single doped samples and (b) $ZnAl_2O_4$ (host) and triple doped samples.

Fig. 8 (a) and (b) shows the Tauc plots for the host, single and triply doped samples, respectively. The Kubelka-Munk function $K = (1 - R)^2/2R$ was used to transform the reflectance to values proportional to absorbance and the Tauc plot of $(K \text{ x } h\nu)^n$ against $h\nu$ (with $n = 2$, which is appropriate for a direct E_g material such as $ZnAl_2O_4$ [27]. The effective E_g is then obtained from the intercept of the linear fit through the horizontal energy axis as illustrated in Fig. 8 (a) and (b). The effective E_g for the Ce^{3+} doped sample was found to be 2.25 eV while it was not an easy task to extrapolate the $h\nu$ values for the host, Tb^{3+} and Eu^{3+} singly doped samples as shown in Fig. 8 (a). Generally, for the triple doped samples it can be seen that the increasing in x% Tb^{3+} ions is accompanied by the slight increase in the effective E_g. These results suggests that the optical E_g of $ZnAl_2O_4$ depends on the dopant type and the concentration of the Tb^{3+} ions on the triple doped samples. Similar observation have been recently reported by Yadav et al. [28] on the Y_2O_3:Tb^{3+}, Bi^{3+} co-doped system. The reason for the slightly lower effective E_g than the E_g of the bulk $ZnAl_2O_4$ (~ 3.8 eV) reported in this study can be explained by considering the diffuse reflection data presented in Fig. 7 (a). From this data, one sees that there is absorption within the E_g of the host material, which is attributed to the defects (and in the case of Ce^{3+} singly doped samples is due to Ce^{3+} ions as indicated above). This narrows the effective optical E_g to be much smaller than that of the foreign ions defect-free $ZnAl_2O_4$. Similar kind of behavior has been observed in $ZnAl_2O_4$:x% Cu^{2+} system and it was termed "shield formation effect" [29]. That is; increasing or populating the E_g defects in $ZnAl_2O_4$ by adding more foreign ions induces the absorbing layer, which absorbs the excited electrons before reaching the conduction band of the host material and as a results this shrinks the bulk $ZnAl_2O_4$ band gap.

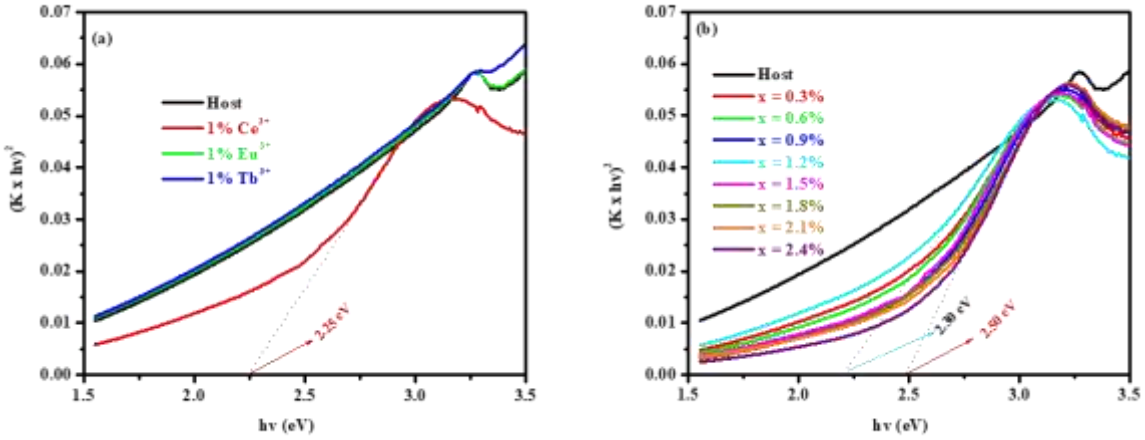

Fig. 8. The Tauc plot for the (a) host, single and (b) triple doped samples.

3.5 Photoluminescence

In order to determine the optimum excitation wavelength for the host sample, various excitation wavelength were used to excite the host sample as shown in Fig. 9 (a). The excitation wavelength as a function of the emission intensity showed the Gaussian behavior as illustrated in Fig. 8 (b). The results suggest that the optimum excitation wavelength for the host sample is 283 nm, which is very close to the excitation wavelength used in ref [29].

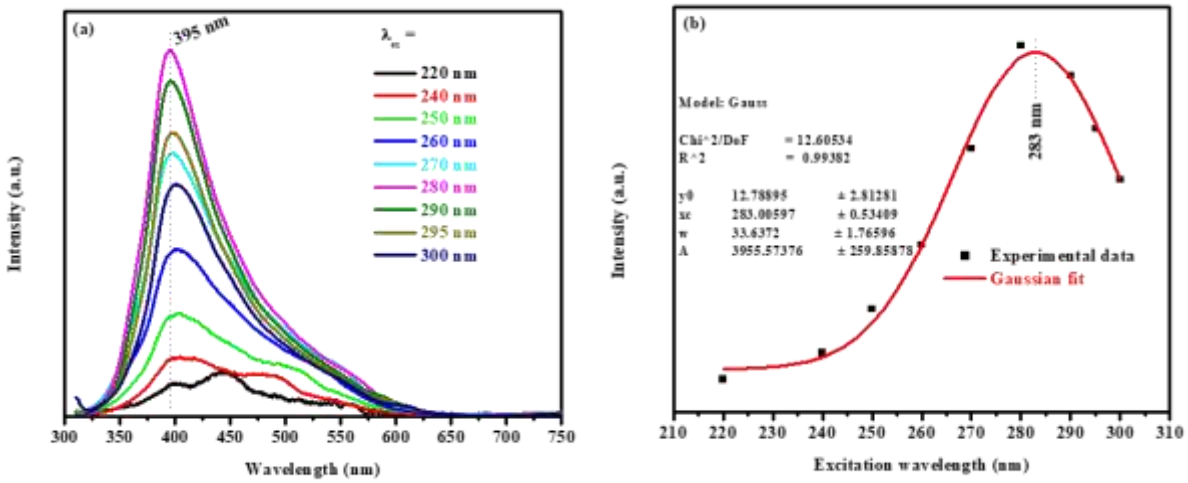

Fig. 9. (a) Host sample excited at different wavelength and (b) excitation wavelength as a function of emission intensity for the host sample.

The room temperature photoluminescence excitation and emission spectra of the host and singly doped 1% Ce^{3+}, 1% $Eu^{3+}$and 1% Tb^{3+} nano-phosphors are shown in Fig. 10 (a). The excitation spectra was carried out when monitoring the emission at 395 nm, which revealed that there are two excitation peaks located around 283 and 328 nm. All of these excitation were attributed to the host material since there was no excitation peak shifts for the single-doped samples and this may also suggest that only the host material was excited. In order to explore the effects of single doping into the host crystal lattice, the singly doped samples were excited at 283 nm. The origin of each emission peaks are clearly shown in details for the host and singly doped samples on the normalized emission spectra in Fig. 10 (b). For the host material, the results revealed a blue emission peak located around 395 nm and this emission was attributed to be from the intrinsic intra-band gap defects within the host material such as oxygen vacancies [10]. Thus, it is emphasized that the emission observed at 395 nm in all samples is due to the host material. The sample doped with Ce^{3+} revealed a broad emission peak with a maximum around 427 nm which was attributed to the electron transition from the 5d lowest energy level of Ce^{3+} to the $^2F_{5/2}$ and $^2F_{7/2}$ manifolds split by spin-orbit coupling. The broadness of the emission spectra is a clear indication that the observed emission originates from more than one energy level [30,31]. Unlike in our previous investigation in $MgAl_2O_4$: Ce^{3+} system [32] where the unfamiliar red emission was observed around 620 nm (5d (e_g) $\rightarrow$ $^4f_1$). In this study, this emission in $ZnAl_2O_4$: Ce^{3+} doped system is yellow-greenish emission observed at 570 nm. The huge shift from 620 to 570 nm can be explained as the adjustment of the crystal field splitting, which shifts the phosphor emission [33]. In addition, Li et al. [34] have observed similar emission on the Ce^{3+}-activated $(Gd, Lu)_3Al_5O_{12}$ garnet solid solutions. Their results further showed that raising the processing temperature from 1000 to 1500 ^oC does not change the emission peak but yielded a 153% increment in the 570 nm emission intensity. Therefore, it is very clear that the emission wavelength depends on the host lattice. The Eu^{3+} singly doped sample showed four distinct emission peaks located around 581, 590, 616 and 654 nm as shown in Fig. 10 (b). These emission peaks were attributed to arise from the $^5D_0 \rightarrow {}^7F_0$, $^5D_0 \rightarrow {}^7F_1$, $^5D_0 \rightarrow {}^7F_2$ and $^5D_0 \rightarrow {}^7F_4$ electronic transitions of Eu^{3+} ion, respectively [35-37]. The Tb^{3+} singly doped sample showed four emission peaks around 490, 545, 588 and 624 nm, which were attributed to the $^5D_4 \rightarrow {}^7F_6$, $^5D_4 \rightarrow {}^7F_5$, $^5D_4 \rightarrow {}^7F_4$ and $^5D_4 \rightarrow {}^7F_3$ electronic transitions from Tb^{3+} ion [9], respectively.

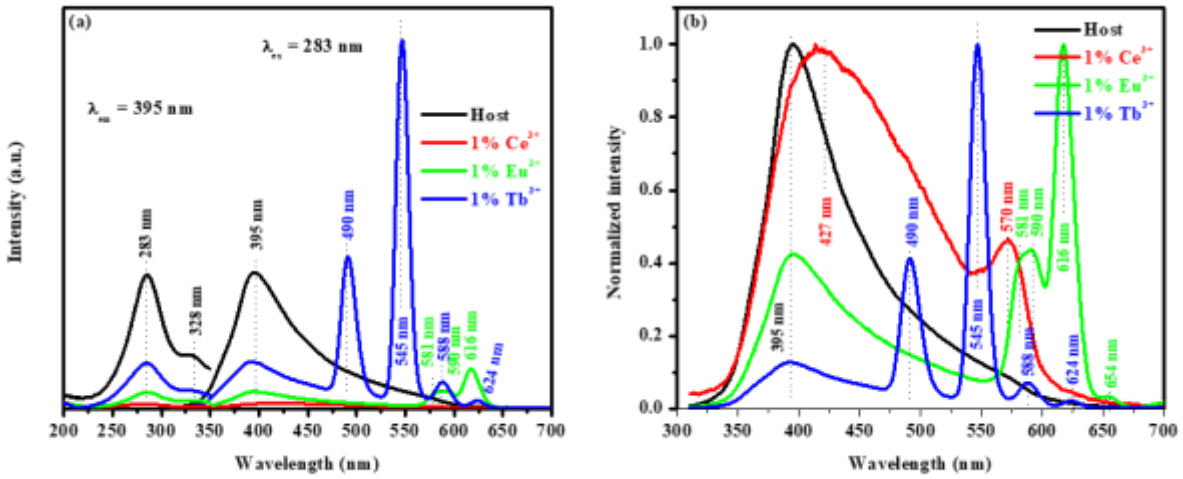

Fig. 10. The PL excitation and emission spectra for the (a) host, single and (b) normalized emission spectra of the singly doped samples.

Fig. 11 shows the comparison of the host and triply doped emission spectra when the samples were excited at 283 nm. The triple doped samples showed similar emissions peaks at around 490, 545, 588 and 616 nm. As discussed in Fig. 10, these emissions are attributed to the Tb^{3+} and Eu^{3+} transitions, respectively. There was no significant observed emission from the host material at 395 nm with an increase with x% Tb^{3+}, which may be suggesting an energy transfer (ET) from the host → Tb^{3+} and possibly from host → Eu^{3+} and lastly from host → Ce^{3+}. Although there is no emission related to the Ce^{3+} ion observed on the triple doped samples (see Fig. 11 (a)), we proposed that the emission from other ions Tb^{3+} and Eu^{3+} suppresses the one from Ce^{3+} as shown in Fig. 10 (a) and (b). In addition, it is important to mention that there is no evidence of ET between the foreign ions. In our previous study [32] on the $MgAl_2O_4$:0.1% Eu^{2+}, 0.1% Ce^{3+}, x% Tb^{3+} triply doped system, there was an ET between the foreign ions, which was from Eu^{2+}→ Tb^{3+} → Ce^{3+}. Zhang et al. [38] observed an ET from Ce^{3+} → Tb^{3+} → Eu^{3+}) in Y_2SiO_5:Ce^{3+}, Tb^{3+}, Eu^{3+} triply doped phosphor. Based on [32,38] results, we therefore conclude that the oxidation state of europium and ET between the foreign ions clearly depends on the host material. Fig. 11 (b) shows the emission intensity (for the 545 nm) as a function of the x% Tb^{3+}, which reveal the linear increase behavior for the investigated Tb^{3+} concentrations.

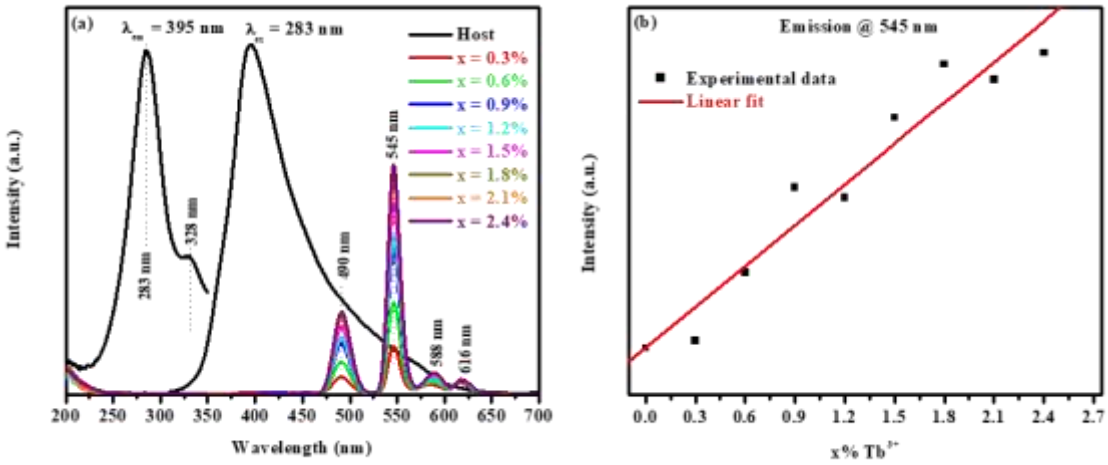

Fig. 11. The excitation and emission spectra for the host and triply doped samples at the varying Tb^{3+} concentration.

Fig. 12 illustrates the proposed emission mechanisms for the observed emissions of the triply doped samples. When electrons (shown by the red cycle) are excited at 283 nm (~ 4.37 eV) from the valence band (VB) of the host material they acquire energy to travel to the conduction band (CB). The excited electrons are de-excited via many channels as shown in Fig. 12, which finally results in distinct emissions from different centers. The excited electrons can also be de-excited via non radiative relaxation (NRR) and trapped into the other defect states or level. Thus, it is clear that the incorporation of the foreign ions into the host matrix can be taken as populating the host material with new extra trapping centers [3]. The location of each RE ion within the host E_g was predicted by using the Dorenbos et al. [39], Rodnyi et al. [40] and Zhang et al. [41] theories, which clearly revealed that the location of each RE ion in numerous hosts material is different.

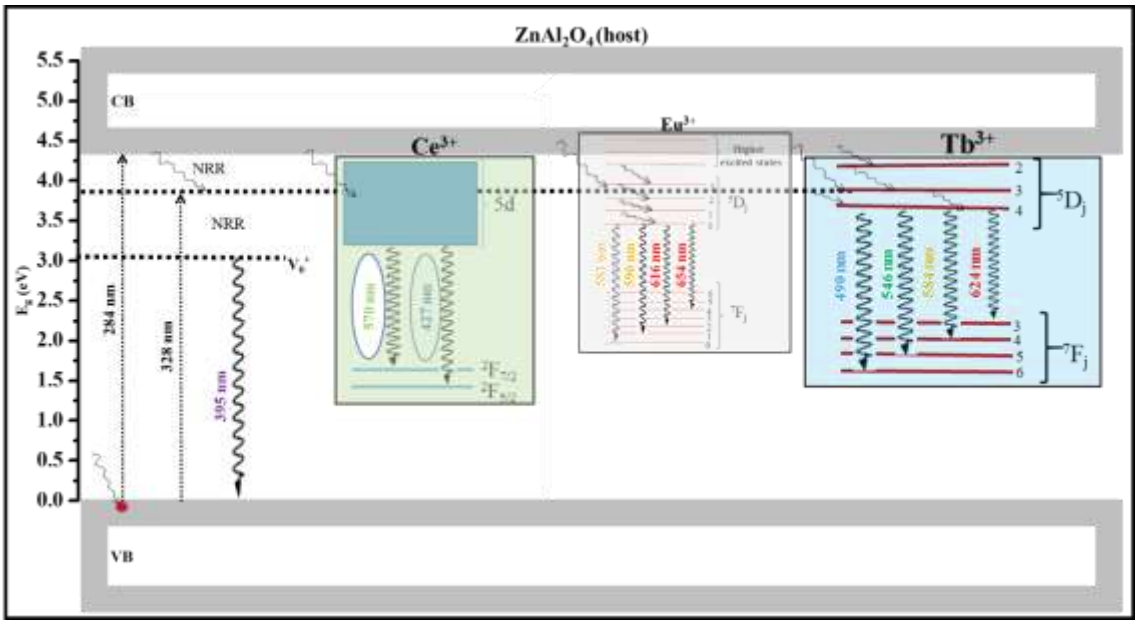

Fig. 12. Emission pathways of the prepared triply doped nano-phosphor.

Fig. 13 shows the excitation spectrum for the 1% Tb^{3+} doped sample for emission at 542 nm, together with emission spectra obtained when exciting at 230 nm, 283 nm and 377 nm. Note that the emission spectrum excited at 377 nm has been scaled to the same intensity as the others. The excitation at 283 nm produces, in addition to the characteristic Tb^{3+} emission peaks, the defect emission band near 395 nm. Often clear f-f excitation bands of Tb^{3+} ions have been reported in excitation spectra in the range 280-380 nm [42], although these are not observed in the present case and the emission spectrum excited at 377 nm shows a strong background of host defect emission, indicating that the host defects are masking this effect. The short wavelength excitation at 230 nm, ascribed to the strong (allowed) f-d excitation transition of Tb^{3+} ions, did not excite the host defect emissions but excited the Tb^{3+} ions to produce an emission spectrum with no background, characteristic of these ions alone. Therefore an excitation wavelength of 230 nm could be used to excite the Tb^{3+} ions directly and was used to investigate their lifetime characteristics, as will be described later.

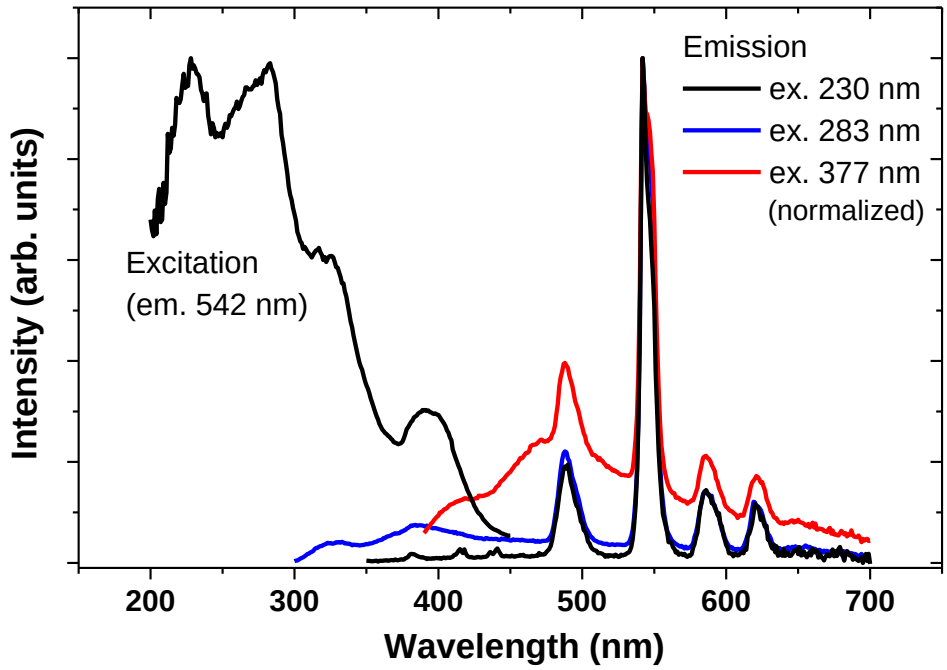

Fig. 13 Excitation and emission of 1% Tb^{3+} doped sample.

Table 2. Summary of the samples identification, decay times, fitting constants and CIE coordinates

Sample ID	τ_1		τ_2		τ_3		τ_{mean} (ms)	CIE	
	Value (ms)	Rel. %	Value (ms)	Rel. %	Value (ms)	Rel. %		*x*	*y*
Host	0.33	23	1.48	48	8.13	29	3.12	0.179	0.160
1% Eu^{3+}	0.29	24	1.36	51	7.84	25	2.71	0.209	0.235
1% Tb^{3+}	0.28	23	1.37	48	8.06	29	3.06	0.422	0.286
1% Ce^{3+}	0.27	28	1.30	44	8.03	28	2.91	0.247	0.500
x = 0.3	0.24	29	1.11	47	7.00	24	2.28	0.348	0.497
x = 0.6	0.24	31	1.05	45	6.50	24	2.10	0.327	0.540
x = 0.9	0.23	31	1.05	47	6.69	22	2.06	0.310	0.559
x = 1.2	0.22	32	1.04	46	6.68	22	2.02	0.303	0.568
x = 1.5	0.26	33	1.00	46	6.37	21	1.85	0.302	0.570
x = 1.8	0.22	34	0.99	46	6.07	20	1.76	0.295	0.577
x = 2.1	0.22	32	1.01	46	6.63	22	2.01	0.297	0.575
x = 2.4	0.23	35	0.98	44	6.56	21	1.90	0.294	0.581

The PL decay curve of the host, singly and triply doped $ZnAl_2O_4$ nanophosphors measured at 283 nm excitation and 395 nm emission characteristic of the host defects are presented in Fig. 14. The third order exponential decay

$$I(t) = A_0 + A_1 e^{\left(-t/\tau_1\right)} + A_2 e^{\left(-t/\tau_2\right)} + A_3 e^{\left(-t/\tau 3\right)} \qquad \ldots (1)$$

where I represents the phosphorescent intensity, A_0 is the background, A_1, A_2 and A_3 are the fitting constants, t is the time of measurement, and τ_1, τ_2 and τ_3 are the components of the decay lifetimes, was used for fitting all the decay curves using the Fluoracle software of Edinburgh Instruments to extract the lifetime components and their relative intensity percentages which are presented in Table 2. The intensity averaged mean life times are in the order of 2-3 ms with strong components (about 20-30%) of the long lifetimes τ_3 of about 6-8 ms. This suggests that there is a persistent luminescence related to the host defects.

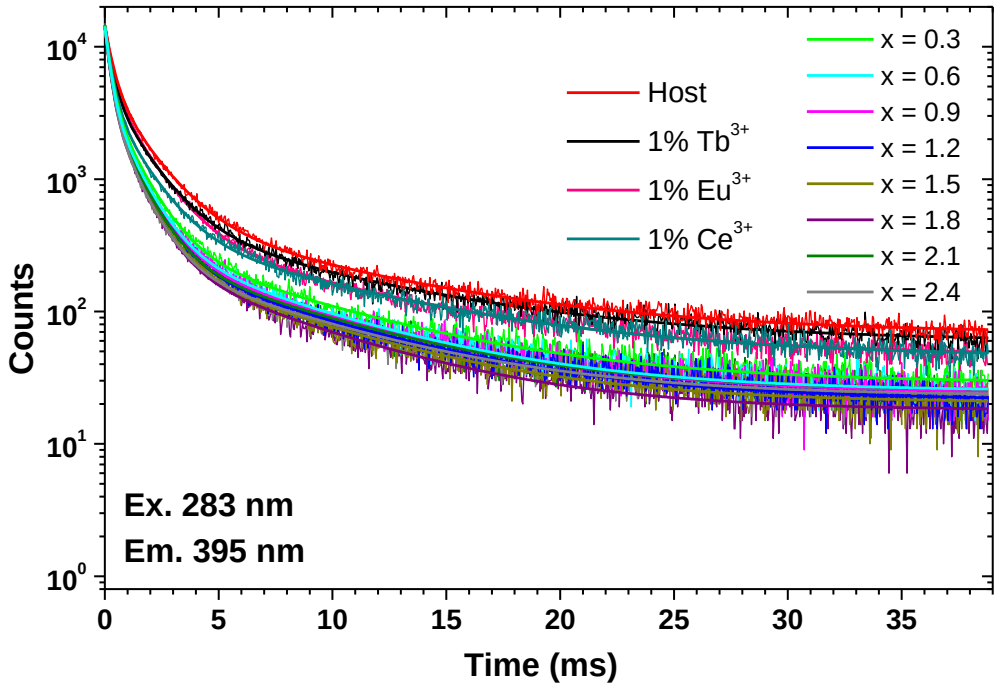

Fig. 14. The decay curves of the defect emission at 395 nm of the $ZnAl_2O_4$ nano-phosphors.

As noted earlier, an excitation wavelength of 230 nm could be used to excite the Tb^{3+} ions without exciting the host defects, and hence it was used to measure the lifetime of the Tb^{3+} $^5D_4 \rightarrow {}^7F_5$ transition at 542 nm. The decay curves are shown in Fig. 15, while the lifetime and fitting constants are presented in Table 3. For the logarithmic intensity scale, the decay curves for the Tb^{3+} ions in Fig. 15 are much straighter than those of the defect emission in Fig. 14. Despite this, best fitting of the decay curves in Fig. 15 still required a triple exponential fitting equation (eq. 1), although the middle lifetime τ_2 in the range 1.3-1.6 ms was dominant with relative component of around 60-70% and the short lifetime component τ_1 made only a small contribution. The existence of three lifetime components suggests three sites for Tb^{3+} ions, or sites

associated with different defects. The mean lifetime of the single doped 1% Tb^{3+} sample was 1.99 ms, while those of the triple doped samples was slightly lower in the range 1.64-1.71 ms and decreased slightly with increasing Tb^{3+} doping concentration, similar to as reported in Ref. [44]. Although the mean lifetime of the host defects (Table 2) and the Tb^{3+} ions (Table 3) are both in the order of milliseconds, they show very different characteristics and fitting components. In the supplementary information the decay curves and fits for emission at 542 nm when excited at 283 nm (the host defect excitation band) and 377 nm, for which the emissions are given in Fig. 13, are provided.

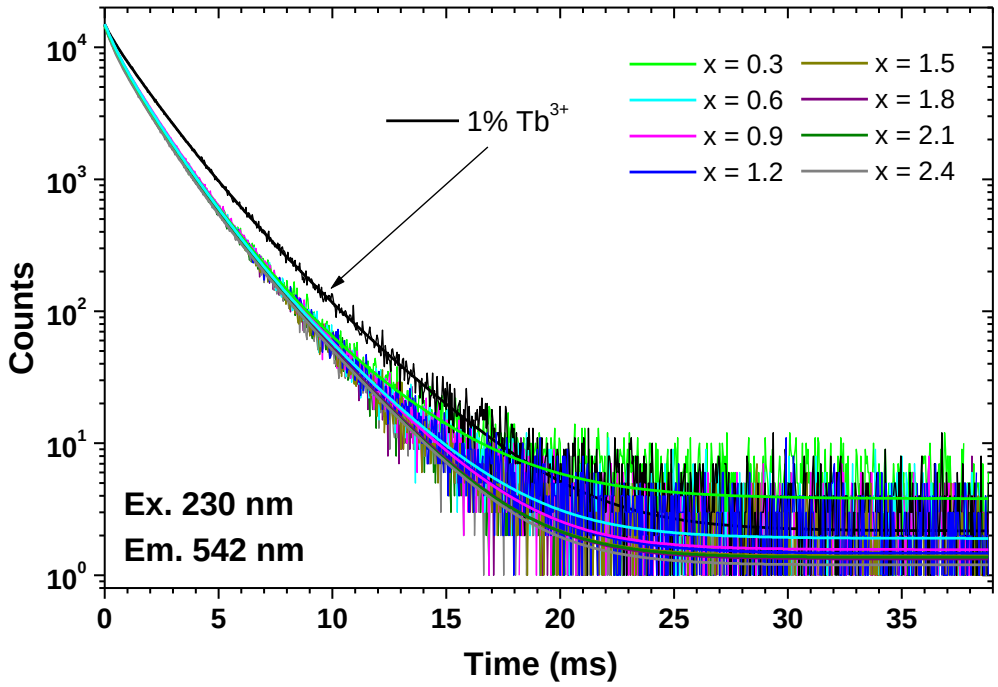

Fig. 15. Decay curves for the 1% Tb doped and triply doped samples excited at 230 nm.

Table 3. The samples identification, decay times and fitting constant for the Tb^{3+} emission at 542 nm and excitation at 230 nm. Lifetime values from the literature are also provided for comparison.

Sample or Ref.	τ_1		τ_2		τ_3		τ_{mean} (ms)
	Value (ms)	Rel. %	Value (ms)	Rel. %	Value (ms)	Rel. %	
1% Tb^{3+}	0.32	2	1.54	62	2.85	36	1.99
x = 0.3	0.59	12	1.58	73	3.27	15	1.71
x = 0.6	0.48	8	1.46	70	2.76	22	1.67
x = 0.9	0.42	6	1.41	65	2.57	29	1.69
x = 1.2	0.41	7	1.38	65	2.63	28	1.67
x = 1.5	0.37	6	1.35	62	2.46	32	1.65
x = 1.8	0.31	5	1.33	62	2.46	33	1.65
x = 2.1	0.42	9	1.38	61	2.49	30	1.64
x = 2.4	0.32	6	1.30	59	2.44	35	1.64
[43]							2.6 - 2.9
[44]							0.42 - 0.93
[45]							~4 - 8.5
[46]							1.34 - 3.1
[47]							2.7 - 2.9

Fig. 16 (a) and (b) illustrates the chromaticity coordinates of the host, singly and triply doped $ZnAl_2O_4$ nano-phosphor. The chromaticity coordinates were determined by the use of the CIE Coordinates calculator software [48]. The software was used to determine the (x;y) co-ordinates and the values presented in Table 2 for each sample prepared. As anticipated the Ce^{3+}, Tb^{3+} and Eu^{3+} singly doped samples emits blue, green and red colour, respectively (see Fig. 16 (a)). Although the main idea for the current study was to synthesis the WLEP, it was generally found that as the Tb^{3+} concentration is increased, the prepared powders emitted the green colour as shown in Fig. 16 (b). The CIE for the x = 2.4% is shown in Fig. 16 (c), which revealed that the emission colour can be tuned by varying the excitation. Thus, further studies are necessary and required to be taken in order to develop the WLEP from the $ZnAl_2O_4$ host material.

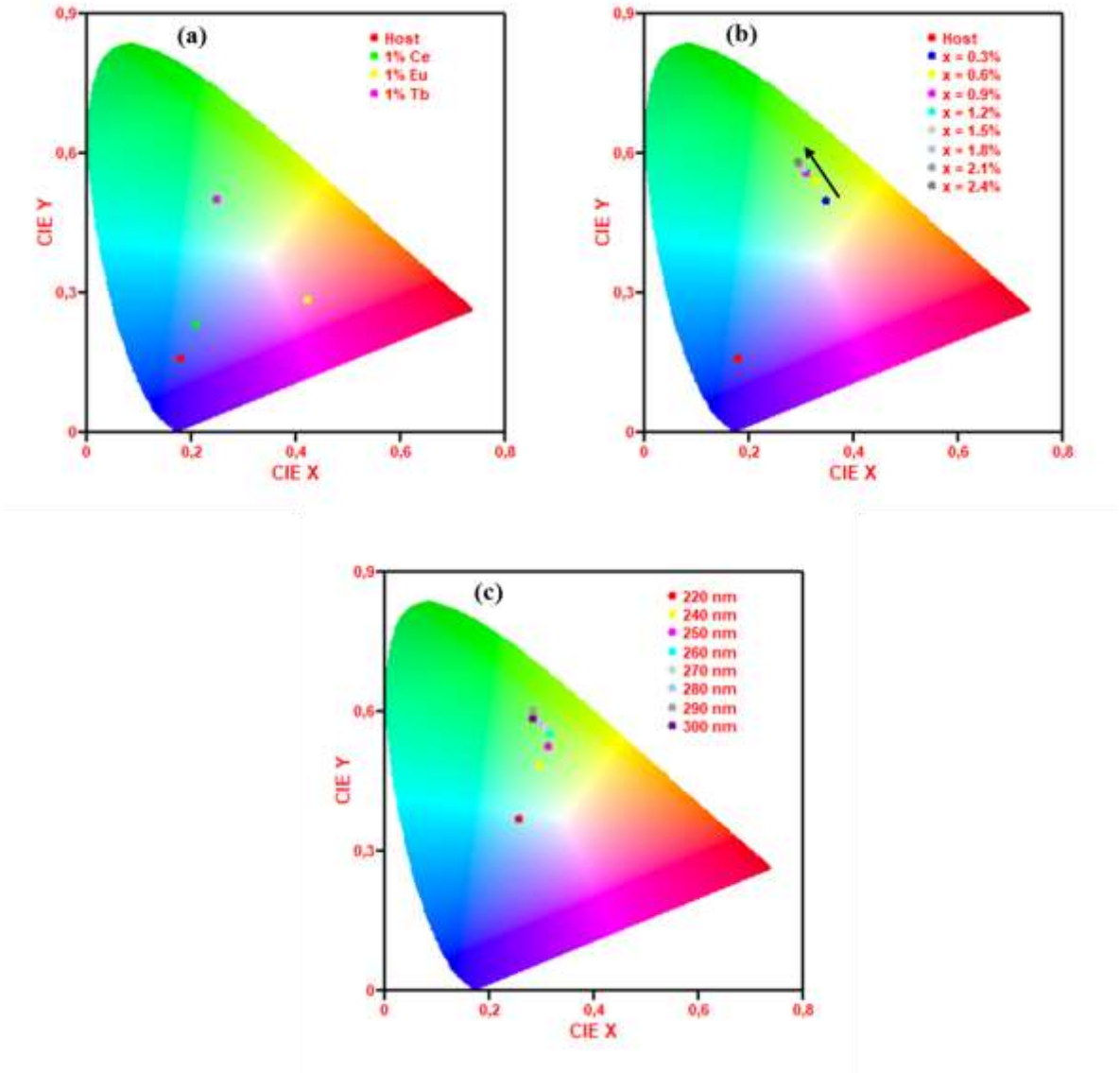

Fig. 16. CIE co-ordinates for the (a) host, singly (b) triply doped $ZnAl_2O_4$ nano-phosphor and (c) x = 2.4 sample excited at various wavelength.

4. Conclusion

$ZnAl_2O_4:Ce^{3+},Eu^{3+},Tb^{3+}$ nano-powders were successfully prepared using the citrate sol-gel method. The XRD data confirmed all the samples consisted of the standard single phase cubic spinel form. The peak intensity, crystallite size, diffraction angle and lattice parameters were influenced by varying the Tb^{3+} concentration. SEM revealed that the prepared samples morphology is also influenced by the dopant type and varying Tb^{3+} concentration. TEM results showed that the prepared powders were in the nanoscale region. PL results showed that the ET occurred from the host → Ce^{3+}, host → Eu^{3+} and host → Tb^{3+} for the singly doped samples. There was no evidence of ET between the foreign ions. The long life times suggests the presence form of persistent luminescence related to the host material defects. CIE color chromaticity confirmed the possibilities of tuning the green emission colour by varying the Tb^{3+} concentration.

Acknowledgements

This work is supported by the South African National Research Foundation (NRF) Thuthuka Programme (fund number: UID99266) and NRF incentive funding for rated researchers (IPRR) (Grant No: 114924). This work is based on the research supported in part by the National Research Foundation of South Africa (R.E. Kroon, Grant Number 93214). The author also acknowledge Mr E. Ndoweni for the sample synthesis.

References

[1] S.K. Sampath, D.G. Kanhere, R. Pandey, Electronic structure of spinel oxides: zinc aluminate and zinc gallate, J. Phys. Cond M. 11 (1999) 3635-3644.

[2] M. Nasr, R. Viter, C. Eid, F. Warmont, R. Habchi, P. Miele, M. Bechelany, Synthesis of novel $ZnO/ZnAl_2O_4$ multi co-centric nanotubes and their long-term stability in photocatalytic application, RSC Adv. 6 (2016) 103692-103699.

[3] V. Ciupina, I. Carazeanu, G. Prodan, Characterization of $ZnAl_2O_4$ nanocrystals prepared by coprecipitation and microemulsion techniques, J. Optoelectron Adv. Mater. 6 (4) (2004) 1317-1322.

[4] J.S. Lee, S. Gupta, P. Kumar, M.B. Ranade, R. Singh, Synthesis and Characterization of YAG:Ce^{3+} Nanophosphor prepared by Flame Spray Pyrolysis, ECS Trans. 16 (30) (2009) 1-6.

[5] W. Wang, S. Kunwar, J.Y. Huang, D.Z. Wang, Z.F. Ren, Low temperature solvothermal synthesis of multiwall carbon nanotubes, J. NanoTech. 16 (2005) 21-23.

[6] B.S. Barros, P.S. Melo, R.H.G.A. Kiminami, A.C.F.M. Costa, G.F. Dosa, S. Alves Jr, Photophysical properties of Eu3+ and Tb^{3+}-doped $ZnAl_2O_4$ phosphors obtained by combustion reaction, J. Mater. Sci. 41 (2006) 4744-4748.

[7] J. Yu, X. Zhao, Q. Zhao, Effect of surface structure on photocatalytic activity of TiO_2 thin films prepared by sol-gel method, Thin Solid Films 379 (2000) 7-14.

[8] S.V. Motloung, M. Tsega, F.B. Dejene, H.C. Swart, O.M. Ntwaeaborwa, L.F. Koao, T.E. Motaung, M.J. Hato, Effect of annealing temperature on structural and optical properties of $ZnAl_2O_4$:1.5% Pb^{2+} nanocrystals synthesized via sol-gel reaction, J. Alloy Comp. 677 (2016) 72-79.

[9] K.G.Tshabalala, S.H. Cho, J.K. Park, S. Shrreyas, I.M. Pilate, R.E. Kroon, H.C. Swart, O.M. Ntwaeborwa, Luminescent properties and X-ray photo electron spectroscopy study of $ZnAl_2O_4$:Ce^{3+},Tb^{3+} phosphor, J. Alloy Comp. 509 (2011) 10115-10120.

[10] S.V. Motloung, F.B. Djene, R.E. Kroon, H.C. Swart, O.M. Ntwaeborwa, Radiative energy transfer in $ZnAl_2O_4$:0.1% Ce^{3+}, x% Eu^{3+} nano-phosphor synthesized by sol-gel process, Physica. B 468-469 (2015) 11-20.

[11] J. PoPović, E. TkalčEc, B. GržETa, S. kuraJica, B. Rakvin, Inverse spinel structure of Co-doped gahnite, Am. Mineral. 94 (2009) 771-776.

[12] S.V. Motloung, F.B. Dejene, H.C. Swart, O.M. Ntwaeaborwa, Effects of Pb^{2+} ions concentration on the structure and PL intensity of Pb-doped $ZnAl_2O_4$ nanocrystals synthesized using sol-el process, J. Sol-Gel Sci. Technol. 70 (2014) 422-427.

[13] A. Fernandez-Osoris, C.E. Rivera, J. Chaves, Europium-Doped ZnAl2O4 Nanophosphors: Structural and Luminescence Properties, Proceedings of the World Congress on New Technologies (2015) 360-366.

[14] I. Omkaram, G. Seeta Rama Raju, S. Buddhudu, Emission analysis of Tb^{3+}:$MgAl_2O_4$ powder phosphor, J. Phys. Chem. Solids 69 (8) (2008) 2066-2069.

[15] T. Chengaiah, C.K. Jcyasankar, L.R. Moorthy, Synthesis and characterization of Ce/Eu co-doped $Na_3Gd(PO_4)_2$ phosphors, Physica B 431 (2013) 137-141.

[16] Y. Wu, J. Du, K. Choy, L.L. Hench, J. Guo, Formation of interconnected microstructural $ZnAl_2O_4$ films prepared by sol-gel method, Thin Solid Films 472 (2005) 150-156.

[17] B.D. Cullity, 2nd Ed., Elements of X-ray Diffraction, 1978, Addison Wesley, 1956, p. 285.

[18] M. Zawadzki, Synthesis of nanosized and microporous zinc aluminate spinel by microwave assisted hydrothermal method (microwave–hydrothermal synthesis of $ZnAl_2O_4$), Solid State Sci. 8 (2006) 14-18.

[19] D.J. Robbins, B. Cockayne, J.L. Glasper, B. Lent, The Temperature Dependence of Rare- Earth Activated Garnet Phosphors II. A Comparative Study of Ce^{3+}, Eu^{3+}, Tb^{3+}, and Gd^{3+} in $Y_3Al_5O_{12}$, J. Electrochem. Soc. Solid-State Sci. Technol. 126 (1979) 1221-1228.

[20] Q. Hou, F. Meng, J. Sun, Electrical and optical properties of Al-doped ZnO and $ZnAl_2O_4$ films prepared by atomic layer deposition, Nano Res. Lett. 8 (2013) 144.

[21] L.F. Koao, F.B. Dejene, R.E. Kroon, H.C. Swart, Effect of Eu^{3+} on the structure, morphology and optical properties of flower-like ZnO synthesized using chemical bath deposition, J. Lumin. 147 (2014) 85-89.

[22] R. Ternane, G. Panzer, M.Th Cohen-Adad, C. Goutaudier, G. Boulon, N. Kbir-Ariguib, M. Trabelsi-Ayedi, Relationships between structural and luminescence properties in Eu^{3+}-doped new calcium borohydroxyapatite, Opt. Mater. 16 (2001) 291-300..

[23] V. Singh, S. Watanabe, T.K. Gunder Rao, J.F.D. Chubaci, I. Ledoux-Rak, H.-Y. Kwak, Infrared luminescence, thermoluminescence and defect centres in Er and Yb co-doped $ZnAl_2O_4$ phosphor, Apply. Phys. B 98 (2010) 165-172.

[24] V. Singh, V.K. Rai, S. Watanabe, T.K. Gundu Rao, L. Badie, I. Ledoux-Kak, Y.-D. Jho, Synthesis, characterization, optical absorption, luminescence and defect centres in Er^{3+} and Yb^{3+} co-doped $MgAl_2O_4$ phosphors, Apply. Phys. 108 (2012) 437-446.

[25] H. Dixit, N. Tandon, S. Cottenier, R. Saniz, D. Lamoen, B. Partoens, V.V. Speybroeck, M. Waroquier, Electronic structure and band gap of zinc spinel oxides beyond LDA: $ZnAl_2O_4$, $ZnGa_2O_4$ and $ZnIn_2O_4$, New J. Phys. 13 (2011) 063002 (11pp).

[26] N. Lakshminarasimhan, U. V. Varadaraju, White-Light Generation in Sr_2SiO_4:Eu^{2+},Ce^{3+} under Near-UV Excitation, J. Electrochem. Soc. 152 (9) (2005) H152-H156.

[27] C. Aydin, M. Benhaliliba, A.A. Al-Ghamdi, Z.H. Gafer, F. El-Tantaway, F. Yakuphanoglu, Determination of optical band gap of ZnO:$ZnAl_2O_4$ composite semiconductor nanopowder materials by optical reflectance method, J. Electroceram. 31 (2013) 265-270.

[28] R.S. Yadav, S.B. Rai, Surface analysis and enhanced photoluminescence via Bi^{3+} doping in a Tb^{3+} doped Y_2O_3 nano-phosphor under UV excitation, J. Alloy Comp. 700 (2017) 228-23.

[29] S.V. Motloung, F.B. Dejene, L.F. Koao, O.M. Ntwaeaborwa, H.C. Swart, T.E. Motaung, O.M. Ndwandwe, Structural and optical studies of $ZnAl_2O_4$:x% Cu^{2+} $(0 < x \leq 1.25)$ nanophosphors synthesized via citrate sol-gel route, Opt. Mat. 64 (2017) 26-32.

[30] S.P. Puppalwar, S.J. Dhoble, G. Singh, A. Kumar, Blue emission in Ce^{3+} and Eu^{2+} activated Lithium fluoro borate phosphors, J. Modern Physics 2 (2011) 1560-1566.

[31] Y. Parganiha, J. Kaur, V. Dubey, K.V.R. Murthy, Near UV-blue emission from Ce doped Y_2SiO_5 phosphor, Materials Science in Semiconductor Processing 31 (2015) 715-719.

[32] S.V. Motloung, B.F. Dejene, O.M. Ntwaeaborwa, H.C. Swart, R.E. Kroon, Colour tuning and energy transfer pathways in $MgAl_2O_4$ triply doped with 0.1% Ce^{3+}, 0.1% Eu^{2+}, x% Tb^{3+} $(0 \le x \le 2\%)$ nanocrystals synthesized using sol-gel process, Chem. Phys. 487 (2017) 75-86.

[33] R. Le Toquin, A.K. Cheetham, Red-emitting cerium-based phosphor materials for solid-state lighting applications, Chem. Phys. Lett. 423 (2006) 352-356.

[34] J. Li, J-G. Li, S. Liu, X. Li, X. Sun, Y. Sakka, The development of Ce3+-activated $(Gd, Lu)_3Al_5O_{12}$ garnet solid solutions as efficient yellow-emitting phosphors, Sci. Technol. Adv. Mater. 14 (2013) 054201 (9pp).

[35] S. Roychowdhury, A.B. Bhattacharya, T Das, A. Singha, M. Manna, J. Apply Eng R. 2 (16) (2015) 1344-1346.

[36] X. Gao, H. Liu, X. Yang, Y. Tian, X. Lu, L. Han, A novel Eu^{3+}/Eu^{2+} co-doped $MgSrLa_8(SiO_4)_6O_2$ single-phase white light phosphor for white LEDs, RSC Adv. 7 (2017) 1711-1717.

[37] J. Zhang, Y. Yang, Y. Liu, C. Mi, G. Li, B. Han, Y. Zhang, H.J. Seo, Photoluminescence Properties of Heavily Eu^{3+}-Doped $BaCa_2In_6O_{12}$ Phosphor for White-Light-Emitting Diodes, J. Am. Ceram. Soc. (2015) 1-7.

[38] X. Zhang, L. Zhou, Q. Pang, J. Shi, M. Gong, Tunable Luminescence and $Ce^{3+} \rightarrow Tb^{3+} \rightarrow Eu^{3+}$ Energy Transfer of Broadband-Excited and Narrow Line Red Emitting Y_2SiO_5:Ce^{3+}, Tb^{3+}, Eu^{3+} Phosphor, J. Phys. Chem. C 118 (2014) 7591-7598.

[39] P. Dorenbos, Electronic structure engineering of lanthanide activated materials, J. Mater. Chem. 22 (2012) 22344-22349.

[40] P.A. Rodny, I.V. Khodyuk, G.B. Stryganyuk, Location of the energy levels of the rare-earth ion in BaF_2 and CdF_2, Phys. Solid State 50 (2008) 1639-1643.

[41] Z-J. Zhang, O.M. Ten Kate, A. Delsing, P. Dorenbos, J-T. Zhao, H.T. Hintzen, Photoluminescence properties of Pr^{3+}, Sm^{3+} and Tb^{3+} doped $SrAlSi_4N_7$ and energy level locations of rare-earth ions in $SrAlSi_4N_7$, J. Mater. Chem. C 2 (2014) 7952-7959.

[42] H.A.A. Seed Ahmed, O.M. Ntwaeaborwa, R.E. Kroon, The energy transfer mechanism in Ce,Tb co-doped LaF_3 nanoparticles, Curr. Appl. Phys. 13 (2013) 1264-1268.

[43] B. Yang, Q. Wang, W. Zhang, S. Ouyang, Y. Zhang, H. Xia, X. Sun, Luminescent properties of Tb^{3+} doped transparent glass ceramics, J. Lumin. 158 (2015) 390-395.

[44] C.R. Kesavulu, A.C.A. Silva, M.R. Dousti, N.O. Dantas, A.S.S. de Camargo, T. Catunda, Concentration effect on the spectroscopic behavior of Tb^{3+} ions in zinc phosphate glasses, J. Lumin. 165 (2015) 77-84.

[45] D. Hreniak, W. Strezk, P. Mazur, R. Pazik, M. Zazbkowska-Wacławek, Luminescence properties of Tb^{3+}:$Y_3Al_5O_{12}$ nanocrystallites prepared by the sol-gel method, Opt. Mater. 26 (2004) 117-121.

[46] Lidia Zur, Marta Sołtys, Joanna Pisarska, Wojciech A. Pisarski, Absorption and luminescence properties of terbium ions in heavy metal glasses, J. Alloys Comp. 578 (2013) 512-516.

[47] Yuya Isokawa, Shotaro Hirano, Naoki Kawano, Go Okada, Noriaki Kawaguchi, Takayuki Yanagida, Radiation-induced luminescence properties of Tb-doped Li_3PO_4-B_2O_3 glasses, Opt. Mater. 76 (2018) 28-33.

[48] ⟨http://www.mathworks.com/matlabcentral/fileexchange/29620-cie-coordinate-calculator⟩ 2012 (accessed 21.10.12).

Supplementary materials

Figure S1 and Table S1 show the decay curves and lifetime fits for the samples excited at 377 nm.

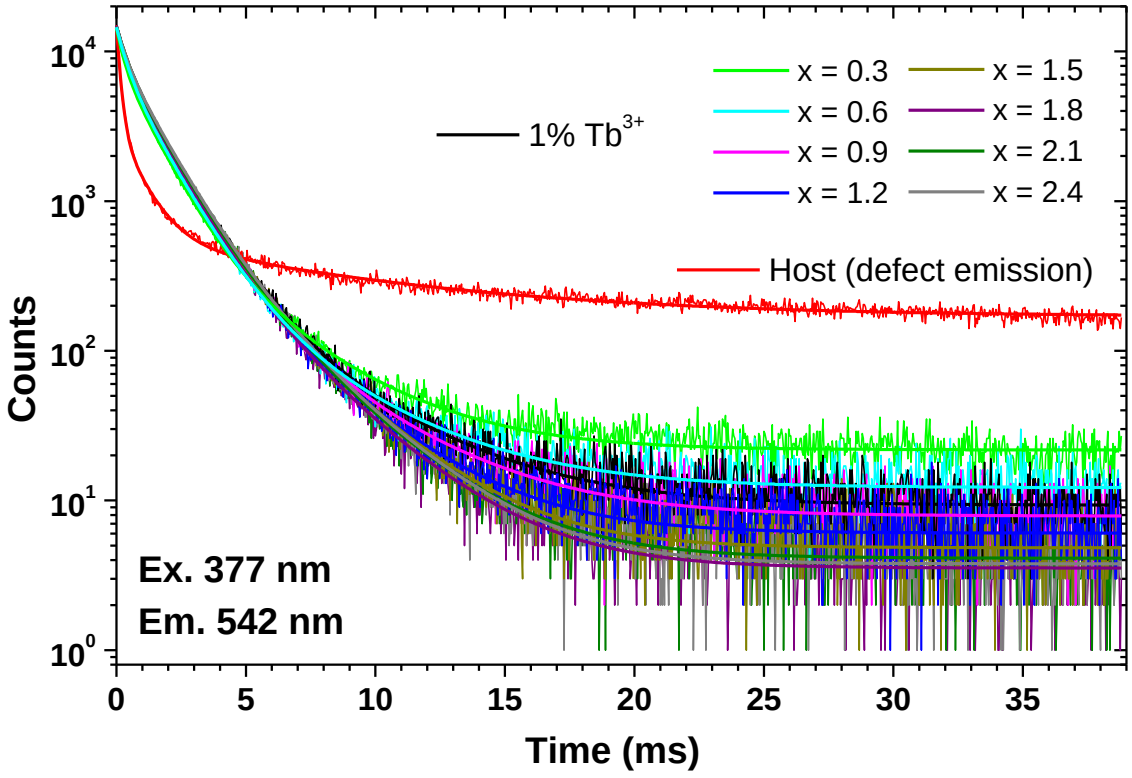

Figure S1.

Table S1.

Sample	τ_1		τ_2		τ_3		τ_{mean} (ms)
	Value (ms)	**Rel. %**	**Value (ms)**	**Rel. %**	**Value (ms)**	**Rel. %**	
Host	0.15	26	0.91	31	8.55	43	3.97
1% Tb^{3+}	0.40	15	1.38	74	3.89	11	1.51
x = 0.3	0.27	13	1.20	69	3.47	18	1.49
x = 0.6	0.37	17	1.33	72	3.93	11	1.46
x = 0.9	0.40	16	1.38	73	3.76	11	1.48
x = 1.2	0.34	13	1.27	72	3.12	15	1.44
x = 1.5	0.33	11	1.25	71	2.88	18	1.46
x = 1.8	0.34	12	1.26	72	2.92	16	1.42
x = 2.1	0.37	13	1.32	72	3.00	15	1.46
x = 2.4	0.35	11	1.29	71	2.88	18	1.48

Figure S2 and Table S2 show the decay curves and lifetime fits for the samples excited at 283 nm.

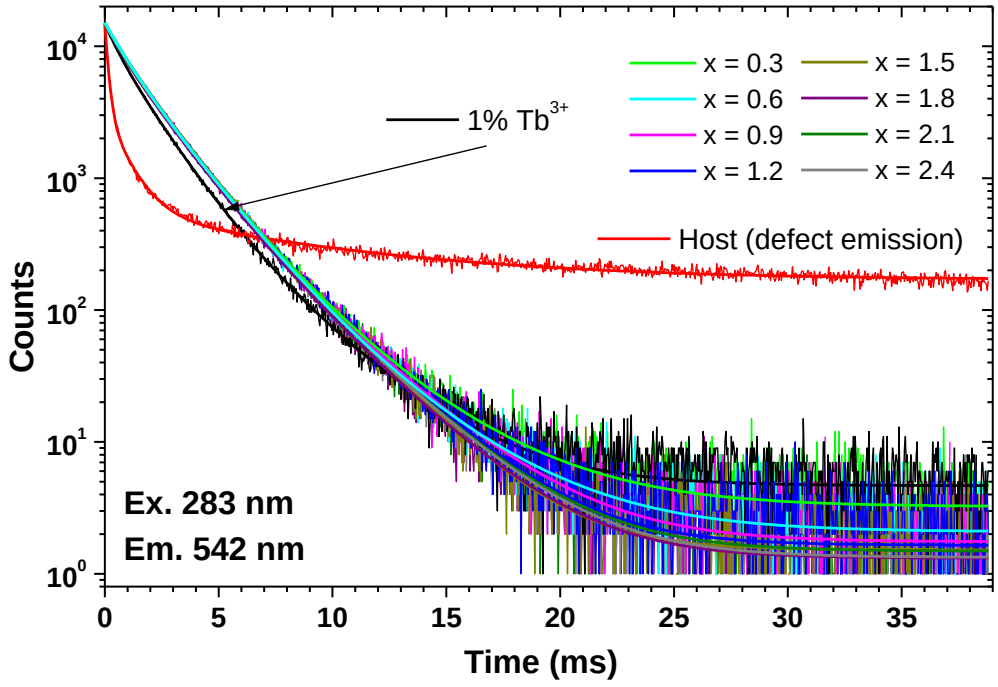

Figure S2.

Table S2.

Sample	τ_1		τ_2		τ_3		τ_{mean} (ms)
	Value (ms)	Rel. %	Value (ms)	Rel. %	Value (ms)	Rel. %	
Host	0.15	26	0.91	31	8.55	43	3.97
1% Tb^{3+}	0.54	9	1.53	73	3.24	18	1.74
x = 0.3	0.90	17	1.92	73	3.92	10	1.93
x = 0.6	0.92	19	1.94	73	3.87	8	1.90
x = 0.9	0.75	9	1.76	73	3.23	18	1.93
x = 1.2	0.58	5	1.57	64	2.86	31	1.91
x = 1.5	0.32	2	1.43	55	2.57	43	1.91
x = 1.8	0.63	7	1.66	69	2.91	24	1.88
x = 2.1	0.61	7	1.72	72	3.03	21	1.92
x = 2.4	0.71	9	1.74	70	3.02	21	1.91